

Semi-Supervised Learning of Monocular Depth Estimation via Consistency Regularization with K-way Disjoint Masking

Jongbeom Baek^{1*} Gyeongnyeon Kim^{1*} Seonghoon Park^{1*} Honggyu An¹
Matteo Poggi² Seungryong Kim^{1†}

¹Korea University, Seoul, Korea ²University of Bologna, Bologna, Italy

{baem0911, kkn9975, seong0905, hg010303, seungryong_kim}@korea.ac.kr m.poggi@unibo.it

Abstract

Semi-Supervised Learning (SSL) has recently accomplished successful achievements in various fields such as image classification, object detection, and semantic segmentation, which typically require a lot of labour to construct ground-truth. Especially in the depth estimation task, annotating training data is very costly and time-consuming, and thus recent SSL regime seems an attractive solution. In this paper, for the first time, we introduce a novel framework for semi-supervised learning of monocular depth estimation networks, using consistency regularization to mitigate the reliance on large ground-truth depth data. We propose a novel data augmentation approach, called K-way disjoint masking, which allows the network for learning how to reconstruct invisible regions so that the model not only becomes robust to perturbations but also generates globally consistent output depth maps. Experiments on the KITTI and NYU-Depth-v2 datasets demonstrate the effectiveness of each component in our pipeline, robustness to the use of fewer and fewer annotated images, and superior results compared to other state-of-the-art, semi-supervised methods for monocular depth estimation. Our code is available at <https://github.com/KU-CVLAB/MaskingDepth>.

1. Introduction

Monocular depth estimation, which aims at estimating a dense depth map from a single image, has been one of the most essential computer vision tasks and can be useful in many fields such as Augmented Reality (AR) [45], Virtual Reality (VR) [33], and autonomous driving [39, 78].

As a pioneering work, Eigen et al. [21] introduced a deep learning-based approach for this task, and several works [37, 46, 66] based on a supervised learning regime

have achieved higher and higher accuracy through the years. However, such a learning paradigm requires a large number of images and corresponding ground-truth dense depths, which are notoriously challenging to obtain [25, 59]. To overcome this, self-supervised learning techniques [28, 29, 82], which formulate monocular depth estimation as an image reconstruction problem, have been popularly proposed. However, these self-supervised methods often require extra data, such as stereo pairs or video sequences [29, 82] which are not always available. In addition, they are known to suffer from scale ambiguity problems and often result in blurred depth at object boundaries and missing instances [5, 14].

On the other hand, to mitigate the reliance on large amounts of labeled data, methods in other fields such as image classification [44, 57, 60] and semantic segmentation [22, 50] have attempted to develop semi-supervised learning frameworks to leverage unlabeled data. Recent successful strategies [8, 60, 62] showed promising performance given very restricted labeled data accompanied with an abundant amount of unlabeled data. Among them, Fix-Match [60] and PseudoSeg [83] in particular showed impressive results by utilizing consistency regularization, a technique that encourages results of strongly-augmented unlabeled data to follow pseudo labels obtained from weakly-augmented unlabeled data.

Compared to other annotations such as image class labels [60] and segmentation labels [83], the cost of obtaining and refining the depth map is much higher and would motivate the need for such techniques, but there has not yet been an attempt to apply SSL approaches for monocular depth estimation. Indeed, adopting the consistency regularization framework to monocular depth estimation is non-trivial. To implement consistency regularization, proper data augmentation is essential, but depth-specific augmentations have rarely been studied [36], and existing techniques have not shown significant effectiveness for monocular depth estimation [34, 36].

In this paper, for the first time, we present a novel semi-

*Equal contribution

†Corresponding author

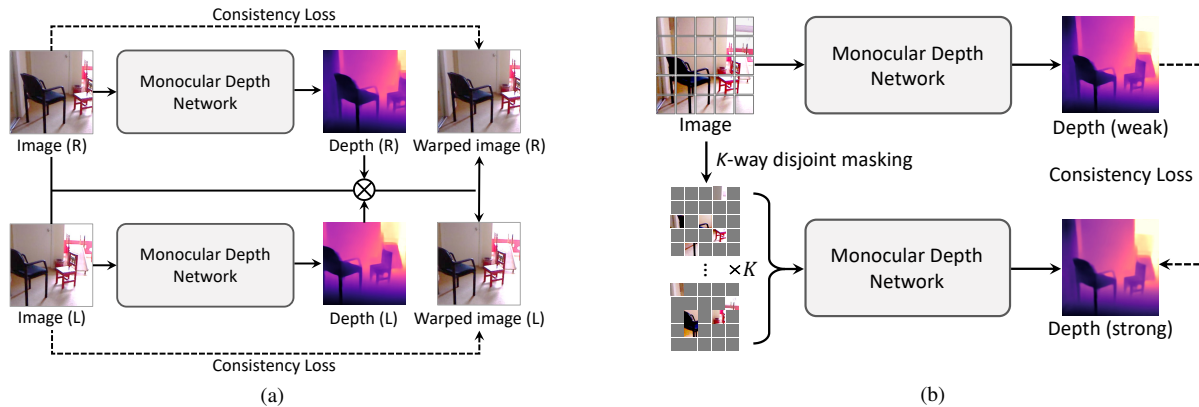


Figure 1. **Motivation:** (a) existing self-supervised methods [24, 28, 29] that enforce consistency between one image and another warped image from stereo or sequential frames, which often results in blurred artifacts and suffers from scale ambiguity problems [10, 67, 68], and (b) our framework that uses consistency regularization by adopting K -way disjoint masking for augmentation, which shows highly improved performance with sparse depth data in a semi-supervised learning setting.

supervised learning framework for monocular depth estimation based on consistency regularization. To apply enough perturbations to an input image in a consistency regularization framework, we propose to adopt a token masking technique as data augmentation, inspired by recent Masked Image Modeling (MIM) strategies for Transformers [6, 32, 74]. Even though MIM yielded superior performance on some tasks, such as image classification and semantic segmentation, naively adopting this as an augmentation technique may increase inherent ambiguity [9, 52] when we estimate the depth of the masked tokens. To overcome this, we present a new approach called K -way disjoint masking as augmentation, where K -disjoint sets of tokens are encoded independently, then concatenated and decoded simultaneously, which helps to generate reliable depth maps while keeping the beneficial effects of masking-based data augmentation. In our framework, we encourage depth and feature consistencies [6] across two branches from two augmented views by K -way disjoint masking. In addition, uncertainty estimation [35, 55] is also jointly modeled to aid the depth consistency and facilitate the convergence of training.

In experiments, we evaluate our framework on standard benchmarks, including KITTI [25] and NYU-Depth-v2 [59]. Our framework shows outstanding performance compared to other semi-supervised monocular depth estimation methods. Especially, our proposed method retains stable performance on sparser label settings. In addition, we show that the proposed K -way disjoint masking is effective as an augmentation technique and validate each component through an extensive ablation study.

2. Related Work

Monocular Depth Estimation. Monocular depth estimation aims at estimating a depth from a single image. [21] pi-

oneering work tackled this task with deep neural networks. Since then, several approaches [46, 66] based on supervised learning, i.e., utilizing ground-truth labels, have been presented to improve performance. Although these methods have achieved remarkable accuracy over traditional, hand-crafted approaches [43, 58], their success depends on massive amounts of ground-truth depth maps that require a labor-intensive process for collection and cleaning [25, 59].

To address this limitation, self-supervised learning methods [24, 29, 72] formulate the task as an image reconstruction, leveraging geometric information over stereo pairs or a sequence of frames. These approaches have emphasized the importance to mitigate the dependency on annotations. However, they often suffer from blurred results [14] and scale inconsistencies when using videos [67, 68]. Unlike both of the aforementioned approaches, there has not been much work on semi-supervised depth estimation. [42] simply combined supervised and self-supervised loss functions and [2] utilized a left-right consistency to improve performance. Recently, several works [13, 31, 64, 71] have attempted to use stereo knowledge to distill labels for monocular depth estimation. Although they seem to be attractive solutions, they are still constrained by the need for specific data (stereo pairs) and additional computation costs (training a stereo module). Our proposed framework alleviates the reliance on labeled data by leveraging consistency regularization which allows us to use unlabeled data.

Semi-supervised Learning. Semi-supervised learning (SSL) [44, 60, 73] has recently emerged as an important area in deep learning. Since collecting labeled data is time-consuming, SSL is a powerful approach to train models on a few annotated samples accompanied by a large amount of unlabeled data. Consistency regularization [3, 44, 57] is one of the commonly used strategies for SSL. It leverages unlabeled data by relying on the assumption that the model

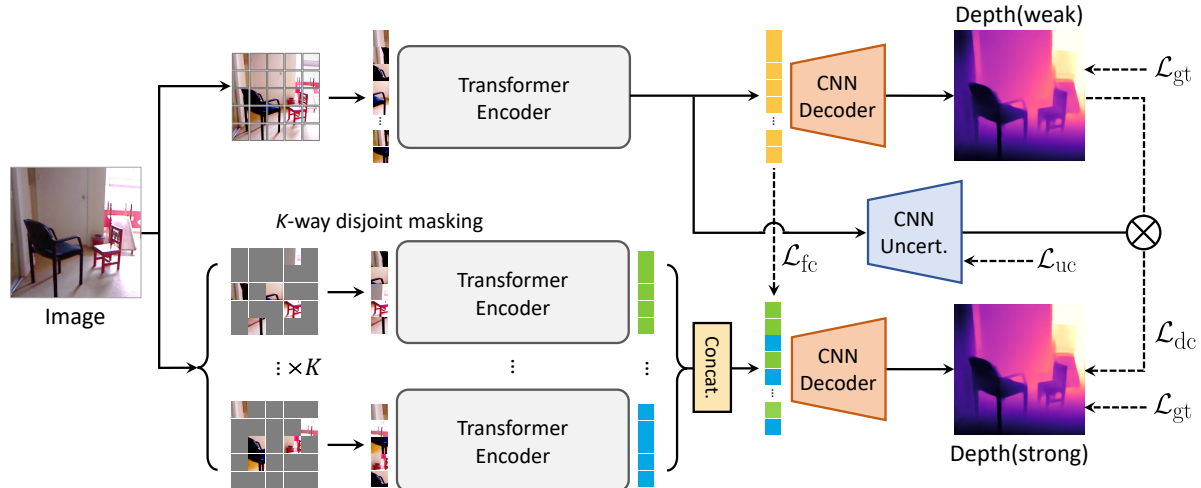


Figure 2. **Overview of the proposed framework.** Our proposed method consists of two main components; a branch using full tokens (top), and a branch using K -way disjoint masked tokens (bottom), where K -number of subsets are encoded independently and concatenated before decoding. We use consistency loss \mathcal{L}_{dc} to make predictions between original and augmented images consistent, aided by an uncertainty measure. Feature consistency loss \mathcal{L}_{fc} is also applied to facilitate the convergence.

outputs should be consistent when perturbations are either applied or not to input samples. Recently, numerous methods [7, 60, 73] that utilize a weakly-augmented image to generate a pseudo-label and enforce consistency against the strongly-augmented image have been proposed. SSL approaches are also used for semantic segmentation [22, 83] to utilize unlabeled data. Inspired by the success of the SSL regime in other fields, we propose a novel semi-supervised framework for monocular depth estimation.

Masked Image Modeling. Masked image modeling is the process of learning representations by reconstructing images that are corrupted by masking [6, 32, 74]. After BERT [17] proposed the masked language modeling tasks, which is one of the successful methods for pre-training in NLP, related works explored a variety of masked image predictions strategies suited for Transformers [6, 32]. ViT [19] studies a masked patch prediction to learn the representation, and BEiT [6] proposes to predict discrete tokens. Recent literature [32, 74] introduce an extremely simple yet effective approach, called masked autoencoder (MAE). MAE [32] only utilizes unmasked tokens to encode meaningful representations. In addition, MRA [75] leverages this strategy to generate augmented images. In this paper, we propose an effective data augmentation strategy tailored for consistency regularization.

3. Methodology

3.1. Motivation and Overview

Let us denote a color image and its corresponding depth map as I and D , respectively. The objective of monocular depth estimation is to learn a mapping function f from

the image I to its corresponding depth D such that $D = f(I)$. Recent learning-based methods formulate the mapping function with convolutions [21, 37, 69] or Transformers [47, 56, 76] as a network f_θ with parameters θ . To train the monocular depth estimation networks f_θ in a supervised manner, the ground-truth $D_{gt}(i)$ defined for all pixels i is required, but building large-scale dense depth data is notoriously challenging [24, 72]. In addition, to alleviate depth capture errors, post-processing [25, 59, 65] is essential.

To overcome this reliance on labeled data, many recent approaches [11, 24, 53, 71, 77, 82] proposed unsupervised or self-supervised learning frameworks, casting the task as an image synthesis problem. Although such self-supervised learning processes mitigate the reliance on labeled data, it often results in blurring results around depth boundaries and failure at accounting for occluded pixels [1, 28]. In addition, it also requires the dataset to consist of stereo pairs or a sequence of frames, which are not always available [25, 59]. In order to combine the complementary advantages of supervised and self-supervised methods, semi-supervised approaches such as combining the two [31, 42] or stereo knowledge distillation [13, 63] have been studied. However, they also have limitations, since posing constraints on the training data composition – needing stereo pairs or sequence images – and additional computation costs for training stereo networks.

In this paper, we present a novel semi-supervised learning framework for learning monocular depth estimation on a large number of unlabeled images with sparsely depth-annotated data. As shown in Fig 1, following recent trends of semi-supervised learning [8, 41, 60, 62], we introduce for the first time consistency regularization between two dif-

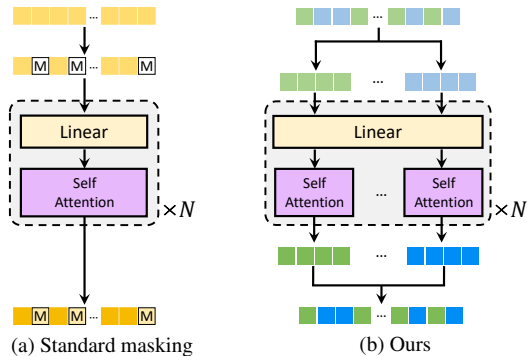


Figure 3. **Illustration of token masking:** (a) standard token masking [6, 74] and (b) our proposed method. Compared to standard masking, our masking strategy consistently well produces dense depth maps because it utilizes the entire set of tokens during decoding.

ferently augmented views from the same image to train the monocular depth estimation network. However, it is challenging to directly apply the existing consistency regularization techniques [44, 49, 57] due to the absence of effective data augmentation for monocular depth estimation. To deal with this, we reformulate this paradigm for our purposes as follows.

3.2. Formulation

Given image I , we formulate two different branches, one for processing images passed through weak augmentation (called weak branch) and the other for images strongly augmented (called strong branch), where the consistency between the two images through the networks f_θ is encouraged. In particular, a weakly-augmented image I_{weak} and a strongly-augmented image I_{strong} are fed to the network f_θ , and then consistency is defined as follows:

$$\mathcal{L} = \mathcal{R}(\text{stopgrad}(f_\theta(I_{\text{weak}})), f_\theta(I_{\text{strong}})), \quad (1)$$

where $\text{stopgrad}(\cdot)$ is a stop-gradient operation and $\mathcal{R}(\cdot, \cdot)$ is a distance function, e.g., mean squared error (MSE) [70] or KL-divergence [38]. In this setting, we can interpret $f_\theta(I_{\text{weak}})$ as a pseudo ground-truth. To effectively implement this strategy, differences between prediction results of divided branches should be made through conventional data augmentation techniques such as crop [18] or rotation [27] which are successfully used in consistency regularization for image classification.

In this framework (as illustrated in Fig 2), following recent successes [56], we consider the backbone model f_θ consisting of a Transformer-based encoder f_θ^{enc} , which takes a tokenized image as input and outputs the encoded features [19], and a CNN-based decoder f_θ^{dec} . However, in monocular depth estimation, if we apply conventional data augmentation techniques such as unconstrained crop [18] or rotation [27], geometric inconsistency due to inherent scale

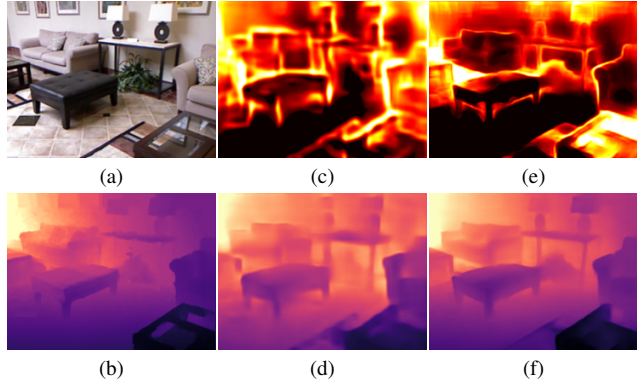


Figure 4. **Examples of estimated depths and uncertainty maps:** (a) RGB, (b) ground-truth depth map, predicted depth maps and their corresponding uncertainty maps by the networks trained with (c), (d) 100 and (e), (f) 10,000 labeled frames and approximately 40,000 unlabeled frames.

ambiguity emerges, and thus the consistency regularization cannot be properly established for our purpose.

To address this issue, we present a novel data augmentation technique tailored to monocular depth estimation, inspired by recent masked image modeling techniques [4, 32, 74], which allows for generating geometrically consistent pseudo depth maps while applying sufficient perturbations to the inputs. In our framework, we encourage not only feature similarities [6] but also depth similarities between the two branches processing the two augmented views, where the latter is aided by uncertainty estimation [35, 55] to ease the convergence of training.

3.3. K -way Disjoint Masking

In this section, we explain how to apply the proposed data augmentation strategy which we call K -way disjoint masking, tailored for consistency regularization in monocular depth estimation. Our key ingredient is inspired by recent MIM techniques for Transformers [6, 32, 74]. The most naive way to formulate this consists of simply masking out the tokens. Specifically, given an image $I \in \mathbb{R}^{h \times w \times 3}$, we reshape it into a sequence of flattened non-overlapped 2D patches $X \in \mathbb{R}^{N \times P}$, where $h \times w$ is the resolution of the original image, $P = p \times p \times 3$ and $p \times p$ is the resolution of each image patch, and $N = hw/p^2$. These flattened 2D patches X are embedded by a trainable linear projection [19] operator, which proceeds to be fed into the Transformer encoder f_θ^{enc} . By applying the randomly sampled mask, the sequence of flattened 2D patches X can be transformed into X' . Note that similar techniques were also used to increase the robustness of Transformers for image-level or pixel-level classification such as segmentation [32, 74]. However, adopting a naive masking strategy for monocular depth estimation is not effective, as we could observe that continuous depth map generation for regions missing

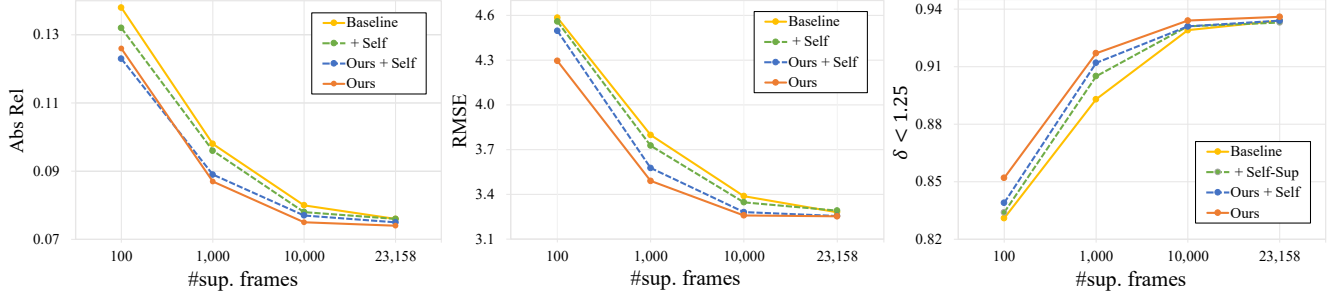


Figure 5. **Quantitative results on the KITTI dataset in a sparsely-supervised setting.** ‘Baseline’ only uses a sparse depth, and ‘Self’ indicates existing self-supervised strategies [24, 29]. ‘Ours’ indicates the proposed semi-supervised learning framework.

from neighboring tokens yields blurred results [52] due to increasing, inherent ambiguity.

To address this, we present a K -way disjoint masking technique, where a K -disjoint set of tokens are encoded independently, then concatenated and decoded simultaneously, as illustrated in Fig 3. Since our method eventually captures the entire scene from the partially divided inputs, it can get deterministic results by reducing inherent ambiguity [52]. Moreover, since it enforces scale consistency by keeping the image size and orientation unaltered, the K -disjoint masking strategy can also act as data augmentation. Specifically, we divide the sequence of flattened 2D patches $X \in \mathbb{R}^{N \times P}$ into K non-overlapping subsets X_k for $k \in \{1, \dots, K\}$, with $X_k \in \mathbb{R}^{M \times P}$, where M is set to be a random value smaller than N to avoid learning with a fixed size of the tokens set. In other words, the concatenation of all the X_k tokens should reconstruct the original token representation X , while keeping the proper position ordering such that

$$X = [X_1, X_2, \dots, X_K], \quad (2)$$

where $[\cdot]$ denotes a concatenation operator. By independently encoding X_k to the latent vector \mathbf{z}_k such that $\mathbf{z}_k = f_{\theta}^{\text{enc}}(X_k)$, unlike original Transformer-based encoding, i.e., $\mathbf{z} = f_{\theta}^{\text{enc}}(X)$, the limited candidates are considered when running self-attention computation, which in turn implements an augmentation over tokens. Then, to decode all the \mathbf{z}_k , we reassemble them as $\bar{\mathbf{z}} = [\mathbf{z}_1, \mathbf{z}_2, \dots, \mathbf{z}_K]$ and obtain the final depth map as $D = f_{\theta}^{\text{dec}}(\bar{\mathbf{z}})$.

In our framework, by adjusting K , we act on the intensity of augmentations to the networks. In our experiments, we empirically set $K = 1$ for the weak branch, and $K = 64$ for the strong branch, which generate decoded depth maps D_{weak} and D_{strong} , respectively.

3.4. Loss Functions

To train the networks we adopt a sparse supervised loss and the proposed unsupervised loss. In addition, we adopt a loss for modeling the uncertainty of the pseudo ground-truth produced by the weak branch and a feature consistency loss. $\|\cdot\|_1$ and $\|\cdot\|_2$ are ℓ_1 and ℓ_2 loss functions, respectively.

Sparse Supervised Loss. When sparse depth-labeled data is available to train the network, we can minimize the supervised loss function \mathcal{L}_{gt} between predicted D and sparse ground-truth D_{gt} such that

$$\mathcal{L}_{\text{gt}} = \|D - D_{\text{gt}}\|_1. \quad (3)$$

In our framework, a small number of fully annotated data used in a supervised manner allows the depth estimation model to ignite the learning process, which is then carried out mainly on unlabeled data through consistency regularization.

Depth Consistency Loss. We formulate a loss that encourages depth prediction of the strongly-augmented image to be close to the prediction of the weakly-augmented image. Since this loss function does not require annotated ground-truths and enables pixel-level learning, it serves as an effective solution to data hunger caused by sparse annotations. The depth consistency loss \mathcal{L}_{dc} assisted by the uncertainty map $U(D_{\text{weak}})$ can be written as:

$$\mathcal{L}_{\text{dc}} = \text{stopgrad}(U(D_{\text{weak}})) \cdot \|\text{stopgrad}(D_{\text{weak}}) - D_{\text{strong}}\|_1. \quad (4)$$

Uncertainty Loss. Ignoring the regions with high uncertainty allows for transferring only the reliable depth knowledge from weak branch to strongly augmented branch. To model such uncertainty, we leverage a negative log-likelihood minimization [35] as

$$L_{\text{uc}} = \frac{\|D - D_{\text{gt}}\|_1}{U(D)} + \log(U(D)), \quad (5)$$

where $U(D)$ denotes the uncertainty map related to the predicted depth map D . By training the network to model its uncertainty, predictions on unlabeled data will be trusted if highly confident, as shown in Fig 4.

Feature Consistency Loss. Within our framework, geometric distortions are not applied to the two branches, and thus the encoded feature consistency can also be encouraged. The feature consistency loss is then defined as

$$\mathcal{L}_{\text{fc}} = \|\mathbf{z}_{\text{weak}} - h(\mathbf{z}_{\text{strong}})\|_2, \quad (6)$$

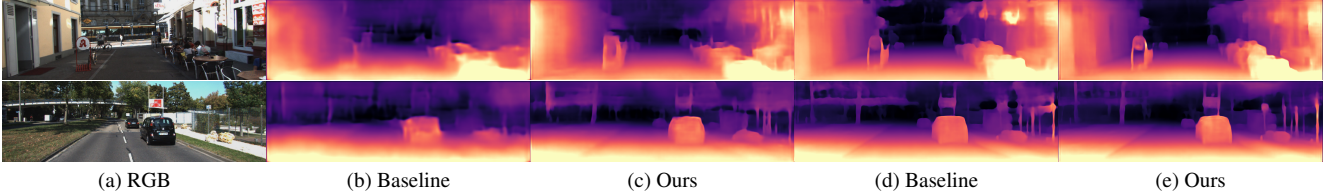


Figure 6. **Qualitative results on the KITTI dataset:** (a) RGB image, predicted depth maps by (b), (d) baseline, and (c), (e) ours using 100 and 10,000 labeled frames, respectively.

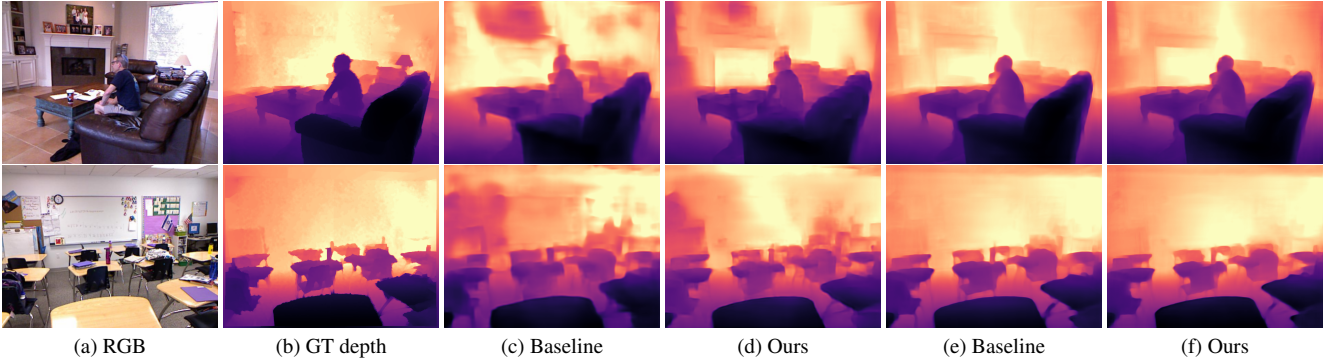


Figure 7. **Qualitative results on the NYU-Depth-v2 dataset:** (a) RGB image, (b) ground-truth depth map, and predicted depth maps by (c), (e) baseline, and (d), (f) ours using 100 and 10,000 labeled frames, respectively.

where $h(\cdot)$ is an additional MLP predictor head, which provides better results as shown in the literature [12, 30] and prevents collapse [79].

Total Loss. By considering all the terms introduced so far, the final loss is defined as

$$\mathcal{L} = \mathcal{L}_{\text{gt}} + \lambda_{\text{uc}}\mathcal{L}_{\text{uc}} + \lambda_{\text{dc}}\mathcal{L}_{\text{dc}} + \lambda_{\text{fc}}\mathcal{L}_{\text{fc}}, \quad (7)$$

where λ_{uc} , λ_{dc} , and λ_{fc} represent weighting parameters.

4. Experiments

4.1. Implementation Details

We implemented our networks with the Pytorch library [51]. We conduct all our experiments with 24GB RTX-3090 GPUs, using DPT [56] as a backbone model. We set the learning rate to 10^{-5} for the encoder and 10^{-4} for the decoder. The encoder is initialized with ImageNet-pretrained [16] weights, whereas the decoder is initialized randomly. We train the entire model with batch size 8 and use Adam optimizer with $\beta_1 = 0.9$ and $\beta_2 = 0.999$.

To avoid collapsing, we balance the ratio of labeled and unlabeled data in one batch to 1:7 similarly to [60]. Besides our new data augmentation approach, we adopt flipping and jittering, widely used in the literature [20, 26]. For confidence estimation, we train the network to predict the log variance because it is more numerically stable [35] than regressing the variance itself, as the loss avoids any division by zero. We use an identical hyperparameter set (i.e., $\lambda_{\text{uc}} = 1$, $\lambda_{\text{dc}} = 1$, $\lambda_{\text{fc}} = 1$, $K = 64$ for strong augmentation) for all experiments unless otherwise specified.

4.2. Experimental Settings

Dataset. We first evaluate the performance of our model and others on the KITTI dataset [25] and NYU-Depth-v2 [59]. KITTI dataset [25] provides outdoor scenes captured by 3D laser data. The RGB images are resized to 640×192 resolutions for training. We follow the standard Eigen training/testing split [21]. We use randomly sampled 10,000, 1,000, and 100 images from $24K$ (i.e., left frames in the Eigen training split) for labeled images during training. We evaluate our trained model on 652 annotated test images for single-view depth estimation, using the improved ground-truth by [65]. NYU-Depth-v2 dataset [59] is composed of various indoor scenes and corresponding depth maps at a resolution of 640×480 . We train our network on the same number of labeled images as KITTI, randomly sampled from the original $40K$ training images. The remaining images in the training set are used as unlabeled images. We test our trained model on 654 test images.

Evaluation Metrics. In our experiments, we follow the standard evaluation protocol of the prior work [21] to evaluate the effectiveness of our framework. The error metrics are defined as Absolute Relative error (AbsRel), Squared Relative error (SqRel), Root Mean Squared Error (RMSE), Root Mean Squared log Error (RMSElog), and accuracy under the threshold (< 1.25) (δ).

4.3. Depth Estimation Results

In this section, we investigate the effects of sparse labels on supervised depth training, and how our proposed semi-supervised learning framework is able to mitigate degrada-

Methods	Sup.	Self.(M)	Self.(S)	Self.	DB.	AbsRel↓	SqRel↓	RMSE↓	RMSElog↓	$\delta\uparrow$
DORN	✓	-	-	-	K	0.072	0.307	2.727	0.120	0.932
BTS	✓	-	-	-	K	0.059	0.241	2.756	0.096	0.959
DPT-Hybrid	✓	-	-	-	K+Mix	0.062	-	2.573	0.092	0.959
DPT-Base*	✓	-	-	-	K	0.074	0.361	3.275	0.117	0.935
Monodepth2	-	✓	✓	-	K	0.080	0.466	3.681	0.127	0.926
PackNet-Sfm	-	✓	-	-	K	0.078	0.420	3.485	0.121	0.931
ManyDepth	-	✓	-	-	K	0.070	0.399	3.455	0.113	0.941
SVSM FT	✓	-	✓	-	K+F	0.077	0.392	3.569	0.127	0.919
Kuznietsov et al.	✓	-	✓	-	K	0.089	0.478	3.610	0.138	0.906
Baek et al.	✓	✓	✓	-	K	0.078	0.381	3.404	0.121	0.930
Guizilini et al.	✓	✓	-	-	K	0.072	0.340	3.265	0.116	0.934
SemiDepth	✓	-	✓	-	K+C	0.078	0.417	3.464	0.126	0.923
Ours (DPT-Base)	✓	-	-	✓	K+C	0.071	0.316	3.049	0.111	0.941

Table 1. **Quantitative results** comparing our method against the existing approaches on the Eigen split of the KITTI dataset, using improved ground truth. ‘Sup.’, ‘Self.(M)’, and ‘Self.(S)’ indicate supervised, existing self-supervised strategies on video and stereo pairs, respectively. ‘Self.’ denotes our proposed consistency regularization, which needs **no stereo images or video sequences**. ‘K’, ‘C’, and ‘F’ indicate KITTI, Cityscapes, and FlyingThings3D, respectively. ‘Mix’ indicate the dataset proposed from [56], which is approximately 60 times larger than KITTI, which contains 1.4M images (DB.). ‘*’ denotes ran by ourselves.

tion in estimated depth maps when the number of labels is significantly limited. This is especially useful for combining vast unlabeled data produced without supervision, with a limited number of labeled data collected independently under more controlled circumstances.

Robustness of Our Framework. As a baseline, we compare DPT-Base [56] trained in supervised and conventional semi-supervised manners obtained with self-supervised losses [24, 29]. Results for the KITTI dataset [25] using different numbers of supervised frames are shown in Fig 5. Our proposed method outperforms the baseline with any different number of data frames. As this amount is decreased further, performance begins to degrade rapidly. This is mostly due to the model’s inability to learn the appropriate scale and structure of the scene with such sparse information. However, as the labels become sparser, the performance degradation of our proposed method progresses more slowly compared to the baseline or naive semi-supervised approach using self-supervised losses, and the performance gap gets larger. Note that when our proposed method is incorporated with the existing self-supervised approach, the performance gain was marginal because the existing solution cannot avoid increasing inherent scale ambiguity from the self-supervised loss function. We also show the qualitative comparison of the baseline and our method on the KITTI dataset in Fig 6 and the NYU-Depth-v2 dataset in Fig 7.

Comparison to Other Methods. As our method does not require any stereo or video sequence frames, it is independent of the configuration of the unlabeled training set. Table 1 shows the result comparing our semi-supervised method with additional data against existing approaches.

Methods	DB.	AbsRel↓	RMSE↓	$\delta\uparrow$
DORN	N	0.115	0.509	0.828
BTS	N	0.110	0.392	0.885
DPT-Hybrid	N+Mix	0.110	0.357	0.904
DPT-Base*	N	0.106	0.380	0.899
Ours (DPT-Base)	N+S	0.104	0.372	0.904

Table 2. **Quantitative results** comparing our method against the existing approaches on the NYU-Depth-v2 dataset. ‘N’ and ‘S’ indicate NYU-Depth-v2 and SUN RGB-D datasets, respectively.

We trained our model on the KITTI dataset [25] as labeled, and the additional Cityscape dataset [15] as unlabeled data. In the results, our method achieves significant improvement in comparison to the baseline by utilizing unlabeled data and surpasses the state-of-the-art in semi-supervised depth estimation methods. Moreover, our method shows competitive performance against DPT-Hybrid, despite smaller model capacity and fewer annotated data being used. A similar trend can be seen in Table 2, where our method utilizes SUN RGB-D [61] dataset as an additional unlabeled dataset and NYU-Depth-v2 as labeled data.

4.4. Ablation Study

For our ablation study, we analyze the effectiveness of different design choices in our framework on KITTI [25]. We exploit 10,000 and 100 randomly sampled images for data augmentation and other ablation studies, respectively.

Data Augmentation. We evaluate our proposed K -way disjoint masking as augmentation in comparison to different MIM methods, including SimMIM [74] and MAE [32], and another data augmentation method, CutOut [18] in either fully supervised or semi-supervised settings with a base-

Method	Sup			Semi-Sup		
	AbsRel ↓	RMSE ↓	$\delta\uparrow$	AbsRel ↓	RMSE ↓	$\delta\uparrow$
Baseline	0.078	3.370	0.930	-	-	-
CutOut	0.076	3.302	0.932	0.075	3.351	0.931
SimMiM	0.077	3.338	0.931	0.076	3.363	0.931
MAE	0.075	3.291	0.933	0.074	3.280	0.934
Ours	0.076	3.289	0.934	0.075	3.239	0.937

Table 3. **Impact of data augmentation.**

Methods	D	U	F	AbsRel ↓	RMSE ↓	$\delta\uparrow$
Baseline	-	-	-	0.136	4.585	0.833
Ours (D)	✓	-	-	0.132	4.355	0.848
Ours (D+U)	✓	✓	-	0.126	4.296	0.851
Ours (F)	-	-	✓	0.131	4.422	0.849
Ours (D+U+F)	✓	✓	✓	0.124	4.263	0.855

Table 4. **Ablation study on main components:** Depth consistency (D), Uncertainty (U), and Feature consistency (F).

line, which is trained in a supervised manner and without any augmentation. The results are summarized in Table 3. Other augmentation methods also improved performance by learning to fill in the missing region, but increase inherent ambiguity. However, our K -way disjoint masking not only reduces the inherent ambiguity by capturing the entire scene but also achieves the best performance.

Loss Functions. We examine each component of the loss function of our method. It consists of four components: sparse supervised term, depth consistency term, feature consistency term, and uncertainty term. Starting with using only sparse supervised loss as the baseline, we study the other three components. As shown in Table 4, the performance of our network improves as each component of the loss function is added. We can see that using all components together leads to a significant improvement.

Predictor Head. To improve the representation power of the encoder, we consider feature consistency loss between encoded features. When the predictor head was removed, collapsing occurred and training did not reach convergence. Our framework without predictor head is conceptually analogous to a naive siamese network, which could not avoid collapsing [79]. In this set of experiments, we evaluate the performance of the predictor head used for providing better results with the feature consistency loss. Results are shown in Table 5. Although using one Transformer block or an MLP showed comparable performance, we use a simple MLP as the default choice for the sake of computational efficiency.

The number of K . To study the influence of the masking ratio, we train the network by adopting different values of K for the strong branch, respectively $K = 4, 16, 64$, and 128. Table 6 shows the quantitative evaluation results for this study. Starting from $K = 4$, the error decreases with

Method	Blocks	AbsRel ↓	$\delta\uparrow$
w/o head	-	0.317	0.423
Transformer	1	0.125	0.856
Transformer	2	0.129	0.848
MLP	2	0.124	0.855

Table 5. **Comparison of using different predictor head.**

K	AbsRel ↓	RMSE ↓	$\delta\uparrow$
$K = 4$	0.131	4.456	0.850
$K = 16$	0.128	4.298	0.855
$K = 64$	0.124	4.263	0.855
$K = 128$	0.132	4.382	0.849

Table 6. **Influence of the number of K .**

Methods	Cap	AbsRel ↓	SqRel ↓	RMSE ↓	RMSElog ↓	$\delta\uparrow$
Kundu <i>et al.</i> [40]	50m	0.203	1.734	6.251	0.284	0.687
T2Net [81]	50m	0.168	1.199	4.674	0.243	0.772
GASDA [80]	50m	0.143	0.756	3.846	0.217	0.836
SharinGAN [54]	50m	0.109	0.673	3.770	0.190	0.864
Ours	50m	0.129	0.719	3.475	0.180	0.845
GASDA [80]	80m	0.149	1.003	4.995	0.227	0.824
SharinGAN [54]	80m	0.116	0.939	5.068	0.203	0.850
Ours	80m	0.136	1.020	4.726	0.190	0.833

Table 7. **Domain adaptation** on the KITTI dataset [25]. For the training data, KITTI dataset [25] and vKITTI dataset [23]. The best results are in **bold**.

the increase of K , until degrading for $K = 128$. We set $K = 64$ as the default since it yields the best results.

4.5. Domain Adaptation

Inspired by [48], we simply apply our framework to unsupervised domain adaptation methods using virtual KITTI (vKITTI) [23] and KITTI [25] as synthetic and real datasets respectively. As demonstrated in Table 7, our framework is lightweight and easily adaptable, yet still achieves reasonable performance compared to generative models.

5. Conclusion

In this paper, we introduced a novel semi-supervised framework for monocular depth estimation using consistency regularization. To this end, we proposed a data augmentation method, called K -way disjoint masking, allowing for leveraging unlabeled data without requiring either stereo or sequential frames. Moreover, the proposed method showed improvement on extremely sparse ground-truth data and superior results compared to other semi-supervised approaches. For future work, we plan to expand our method to other dense prediction tasks.

Acknowledgements. This research was supported in part by Autonomous Driving Center, R&D Division, Hyundai Motor Company.

Appendix

In this appendix, we provide more results on experiments carried out and more implementation details of our framework.

Appendix A. More Quantitative Results

More detailed quantitative results of our proposed method and conventional self-supervised method on KITTI dataset [25] are shown in Table 8. Moreover, to verify generalization ability of our framework, we evaluated our framework on NYU-Depth-v2 dataset [59]. Results are shown in Table 9.

Methods	# sup. frames	AbsRel ↓	SqRel ↓	RMSE ↓	RMSElog ↓	$\delta\uparrow$
Baseline	23,158	0.076 ± 0.003	0.365 ± 0.004	3.290 ± 0.015	0.118 ± 0.001	0.934 ± 0.001
	10,000	0.079 ± 0.001	0.379 ± 0.007	3.388 ± 0.019	0.121 ± 0.009	0.929 ± 0.001
	1,000	0.098 ± 0.004	0.515 ± 0.030	3.785 ± 0.013	0.142 ± 0.005	0.899 ± 0.005
	100	0.135 ± 0.005	0.728 ± 0.019	4.585 ± 0.048	0.186 ± 0.011	0.831 ± 0.005
	10	0.201 ± 0.023	1.508 ± 0.045	6.163 ± 0.082	0.268 ± 0.029	0.701 ± 0.021
Baseline + Self.(M)	23,158	0.076 ± 0.002	0.367 ± 0.007	3.291 ± 0.020	0.117 ± 0.001	0.933 ± 0.002
	10,000	0.078 ± 0.001	0.376 ± 0.006	3.347 ± 0.043	0.119 ± 0.002	0.931 ± 0.001
	1,000	0.096 ± 0.002	0.523 ± 0.024	3.750 ± 0.033	0.140 ± 0.002	0.900 ± 0.004
	100	0.132 ± 0.004	0.759 ± 0.014	4.559 ± 0.044	0.184 ± 0.003	0.834 ± 0.004
	10	0.210 ± 0.020	1.322 ± 0.042	5.627 ± 0.080	0.265 ± 0.027	0.711 ± 0.016
Ours+Self.(M)	23,158	0.079 ± 0.001	0.379 ± 0.007	3.388 ± 0.019	0.121 ± 0.009	0.929 ± 0.001
	10,000	0.076 ± 0.017	0.369 ± 0.004	3.311 ± 0.011	0.117 ± 0.001	0.935 ± 0.002
	1000	0.085 ± 0.017	0.430 ± 0.011	3.521 ± 0.012	0.129 ± 0.012	0.918 ± 0.010
	100	0.123 ± 0.003	0.747 ± 0.018	4.497 ± 0.042	0.181 ± 0.005	0.839 ± 0.005
	10	0.184 ± 0.011	1.265 ± 0.064	5.747 ± 0.080	0.243 ± 0.007	0.727 ± 0.018
Ours	23,158	0.074 ± 0.001	0.362 ± 0.001	3.253 ± 0.012	0.116 ± 0.001	0.935 ± 0.001
	10,000	0.075 ± 0.002	0.362 ± 0.006	3.259 ± 0.020	0.116 ± 0.001	0.934 ± 0.003
	1,000	0.088 ± 0.003	0.419 ± 0.007	3.490 ± 0.020	0.129 ± 0.003	0.917 ± 0.002
	100	0.128 ± 0.004	0.707 ± 0.013	4.295 ± 0.037	0.173 ± 0.006	0.849 ± 0.006
	10	0.197 ± 0.019	1.378 ± 0.032	5.650 ± 0.091	0.261 ± 0.030	0.723 ± 0.017

Table 8. **Quantitative results** on the KITTI dataset [25] in a sparsely-supervised setting using sparse labels from [65]. For each row, we trained 5 independent models with randomly selected labels from entire dataset to calculate the mean and variance. ‘Self.(M)’ and ‘Ours’ indicate monocular self-supervised learning and proposed consistency regularization, respectively. The best results are in **bold**.

Methods	# sup. frames	AbsRel ↓	RMSE ↓	log ₁₀ ↓	δ↑
Baseline	42,602	0.106 ± 0.002	0.380 ± 0.004	0.053 ± 0.001	0.897 ± 0.001
	10,000	0.112 ± 0.004	0.389 ± 0.006	0.057 ± 0.003	0.893 ± 0.003
	1,000	0.141 ± 0.008	0.447 ± 0.009	0.066 ± 0.004	0.843 ± 0.006
	100	0.199 ± 0.011	0.604 ± 0.014	0.086 ± 0.005	0.694 ± 0.011
	10	0.321 ± 0.040	0.872 ± 0.042	0.124 ± 0.008	0.523 ± 0.027
Ours	42,602	0.105 ± 0.002	0.379 ± 0.003	0.053 ± 0.001	0.899 ± 0.001
	10,000	0.107 ± 0.002	0.386 ± 0.006	0.054 ± 0.002	0.896 ± 0.002
	1,000	0.135 ± 0.007	0.440 ± 0.008	0.065 ± 0.004	0.853 ± 0.005
	100	0.182 ± 0.008	0.594 ± 0.012	0.083 ± 0.003	0.718 ± 0.010
	10	0.292 ± 0.031	0.814 ± 0.037	0.112 ± 0.006	0.561 ± 0.021

Table 9. **Quantitative results** on the NYU-Depth-v2 dataset [59] in a sparsely-supervised setting. For each row, we trained 5 independent models with randomly selected labels from entire dataset to calculate the mean and variance.

Appendix B. More Qualitative Results

In the main paper, we have visualized the comparisons of baseline and our methods on NYU-Depth-v2 dataset [59] and KITTI dataset [25]. In this section we provide additional qualitative results after having trained on 100 and 10,000 frames in Fig 8 and Fig 9. Our method shows better results, especially at semantic level and object boundaries, while the baseline approach shows poor result on them.

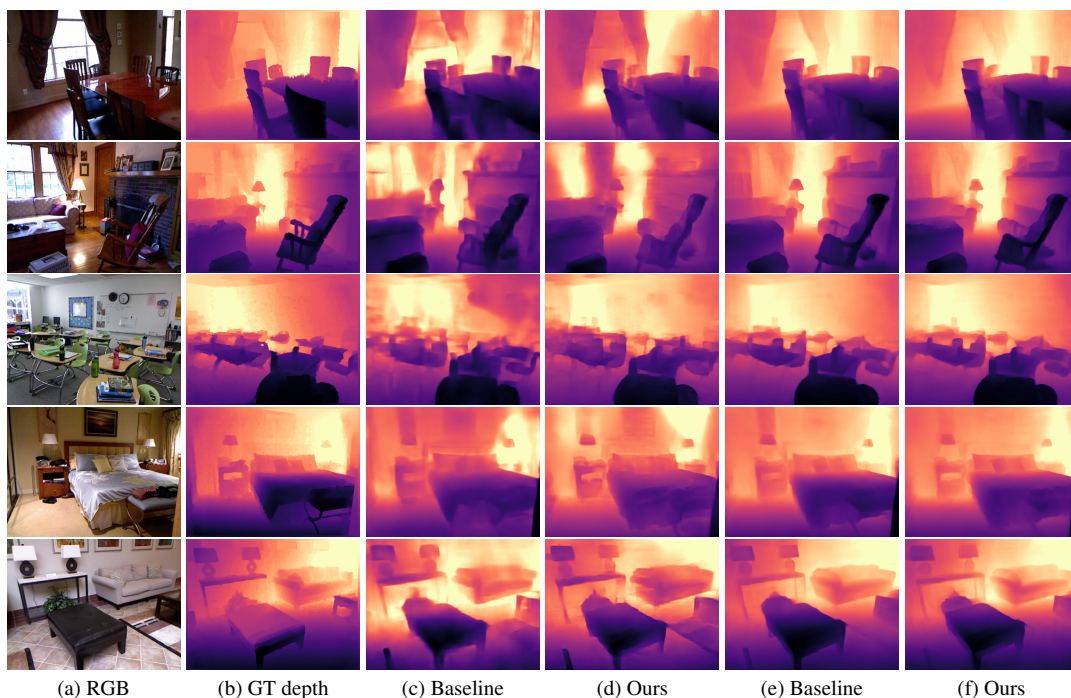


Figure 8. **Qualitative results on the NYU-Depth-v2 dataset [59]:** (a) RGB image, (b) ground-truth depth map, and predicted depth maps by (c), (e) baseline, and (d), (f) ours using 100 and 10,000 labeled frames, respectively.

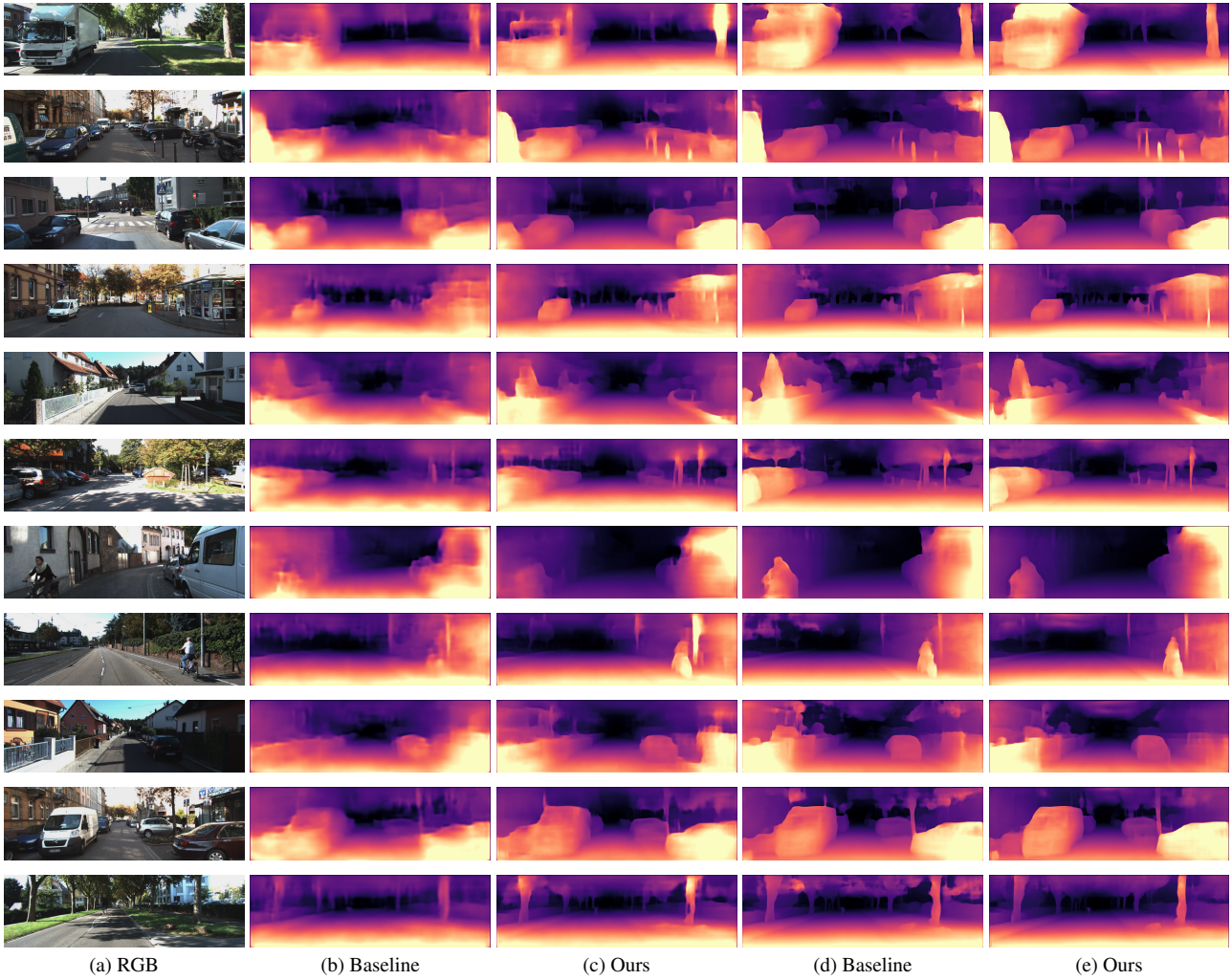


Figure 9. **Qualitative results on the KITTI dataset [25]:** (a) RGB image, (b) ground-truth depth map, and predicted depth maps by (c), (e) baseline, and (d), (f) ours using 100 and 10,000 labeled frames, respectively.

Appendix C. More Implementation Details

PyTorch-like Pseudo-code for K -way disjoint masking modeling. We provide pseudo-code for K -way disjoint masking modeling, in order to show how our novel technique can be implemented independently. This enables the effect of data augmentation while preserving the geometry.

Algorithm 1: Pseudo Code of K -way disjoint masking modeling

```
1 # Input: Transformer are basic transformer encoder blocks
2 # Input: X (B x N x P) is patch embeddings
3 # where N is number of patches and P is embedding dimension
4 # Input: K is number of masking subsets.
5 # Output: Z (B x N x P) is K-way disjointly encoded features
6 def K_way_masked_transformer(transformer, X, K):
7     B, N, _, _ = X.shape
8
9     batch_range = torch.arange(B)[: , None]
10    rand_indices = torch.rand(B, N).argsort(dim = -1)
11    X = X[batch_range, rand_indices]
12    # patch wise random shuffling on X
13    # X is no longer spatial order after shuffling
14
15    v = sorted([random.randint(1, N-1) for i in range(int(K-1))] + [0, N])
16    # sampling subset split point randomly
17    mask_v = torch.zeros(len(v[:-1]), N)
18    for i in range(len(v[:-1])):
19        mask_v[i, v[i]:v[i+1]] = 1.0
20
21    attention_mask = mask_v.transpose(0,1) @ mask_v
22    # mask has shape of (B x N x N)
23    # attention matrix masking from different subset
24    # by applying this attention mechanism proceeds semi-globally
25
26    Z_ = transformer(x, attention_mask)
27    # Z (B x N x P) is K-way masked token embeddings
28    reform_indices = torch.argsort(rand_indices, dim=1)
29
30    return Z_[batch_range, reform_indices]
31    # reassemble features to spatial order and return
32
33
34 # In the transformer, attention method
35 # Input: Q, K, V (B x N x P) is Query, Key, Value vectors
36 # Input: mask (B x N x N) attention mask
37 # Output: V' (B x N x P) mask attentioned Value vectors
38 def attention(Q, K, V, mask):
39     dots = torch.matmul(Q, K.transpose(-1, -2)) * sqrt(Q.shape[-1])
40     ## general attention matrix that has shape of (B x N x N)
41
42     if not(mask == None):
43         dots[:, :, mask==0.0] = -10.0
44     ## replace value of masked region with negatives befor softmax
45     ## so it's attention distribution value goes nearly zero after softmax
46
47     attn = Softmax(dots, dim=-1)
48     V = torch.matmul(attn, V)
49
50     return V
```

PatchEmbedding		
Layer	Parameters (in, out, k, s, p)	Output shape ($C \times H \times W$)
Conv	(3, 768, 16, 16, 0)	(768, 12, 40)
Rerange	-	($HW = 480, C = 768$)
Transformer Encoder N blocks		
Layer	Parameters (in, out)	Output shape (C)
LayerNorm	-	(768)
Linear-N-1	(768, 2304)	(2304)
Attention	-	(768)
Linear-N-2	(768, 768)	(768)
LayerNorm	-	(768)
Linear-N-3	(768, 3072)	(3072)
GELU	-	(3072)
Linear-N-4	(3072, 768)	(768)
Decoder		
Layer	Parameters (in, out, k, s, p)	Output shape ($C \times H \times W$)
Conv-1(Linear-2-4)	(768,96,1,1,0)	(96,12,40)
ConvTranspose-1	(96,96,4,4,0)	(96,48,160)
Conv-2	(96,256,3,1,1)	(256,48,160)
Conv-3(Linear-5-4)	(768,192,1,1,0)	(192,12,40)
ConvTranspose-2	(192,192,2,2,0)	(192,24,80)
Conv-4	(192,256,3,1,1)	(256,24,80)
Conv-5(Linear-8-4)	(768,384,1,1,0)	(384,12,40)
Conv-6	(384,256,3,1,1)	(256,12,40)
Conv-7(Linear-11-4)	(768,768,1,1,0)	(768,12,40)
Conv-8	(768,768,3,2,1)	(768,6,20)
Conv-9	(768,256,3,1,1)	(256,6,20)
Fusion(x)		
Layer	Parameters (in, out, k, s, p)	Output shape ($C \times H \times W$)
ReLU	-	(256,h,w)
Conv-10	(256,256,3,1,1)	(256,h,w)
ReLU	-	(256,h,w)
Conv-11	(256,256,3,1,1)	(256,h,w)
ReLU	-	(256,h,w)
Fusion-1(Conv-9)	-	(256,6,20)
UpSample	-	(256,12,40)
Conv-12	(256,256,1,1,1)	(256,12,40)
Fusion-2(Conv-6)	-	(256,12,40)
add-2(Fusion-2,Conv-12)	-	(256,12,40)
Fusion-4(add-2)	-	(256,12,40)
UpSample	-	(256,24,80)
Conv-13	(256,256,1,1,1)	(256,24,80)
Fusion-5(Conv-4)	-	(256,24,80)
add-3(Fusion-5,Conv-13)	-	(256,24,80)
Fusion-6(add-3)	-	(256,24,80)
UpSample	-	(256,48,160)
Conv-14	(256,256,1,1,1)	(256,48,160)
Fusion-7(Conv-2)	-	(256,48,160)
add-4(Fusion-7,Conv-14)	-	(256,48,160)
Fusion(add-4)	-	(256,48,160)
UpSample	-	(256,96,320)
Conv-15	(256,256,1,1,1)	(256,96,320)
Conv-16	(256,128,3,1,1)	(128,96,320)
UpSample	-	(256,192,640)
Conv-17	(128,32,3,1,1)	(32,192,640)
ReLU	-	(32,192,640)
Conv-18	(32,1,1,1,0)	(1,192,640)
sigmoid	-	(1,192,640)

Table 10. Network architecture of our model.

Network Architecture Details. We summarize the detailed network architecture of our model in Table 10. Our encoder basically follows ViT [19] without class token. We use 12 transformer blocks(ViT-Base) and extract features 2, 5, 8, and 11 for skip connection input ($0 \leq N \leq 11$). The Decoder structure follows DPT [56], and the Decoder part in the Table 10 indicates 4 skip connections. However there are no readout operations, because no class token is used.

Appendix D. Qualitative Results of Domain Adaptation

In our main paper, we demonstrated that our framework is lightweight, easy to use for domain adaptation, and has reasonable performance compared to other techniques. We also show the qualitative results of our domain adaptation experiments in Fig 10.

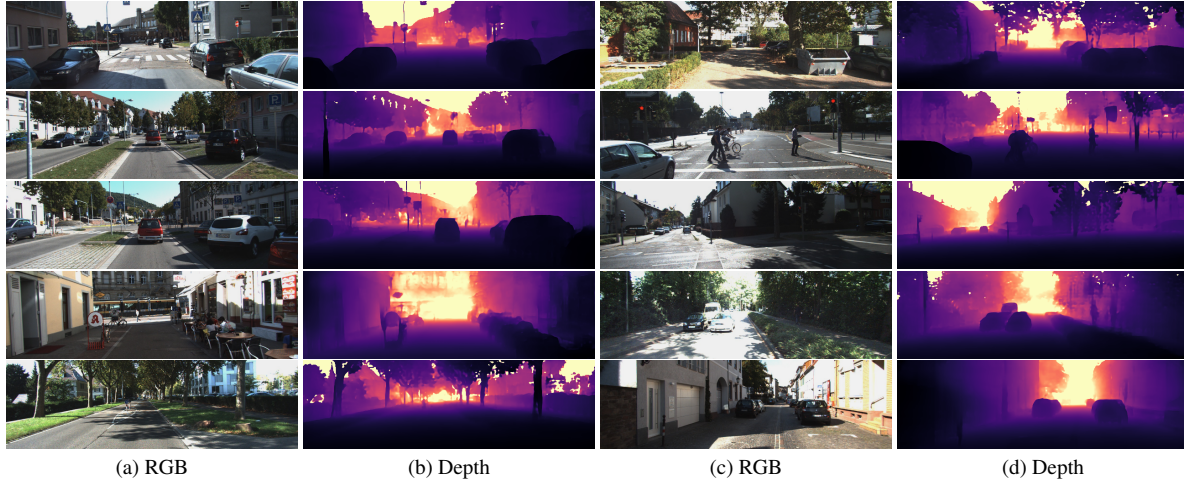


Figure 10. **Qualitative results on the KITTI dataset [25]:** (a), (c) RGB image, and (b), (d) depth map. Our framework proves to work well in domain adaptation task on real-world images.

Appendix E. Limitations and Broader Impact

Limitations. In this paper, we introduce a novel framework semi-supervised depth estimation method using consistency regularization. However, our approach learns unlabeled data by following the guidance of a small number of labeled data, so it may fail to predict depth in sparse annotations such as sky regions. Another limitation is that our method performs well on the KITTI dataset [25], while the performance improves relatively less on images with a higher variety of content, e.g., as in the NYU-Depth-v2 dataset [59].

Broader Impact. In the future, we aim to apply our method in various data domains, and develop the performance of our framework by leveraging the newly studied data augmentation techniques. Our work is an essential study in order to be completely free from the dependence of the data, and provides the possibility to replace the existing self-supervised methods requiring additional images.

References

- [1] Aitor Alvarez-Gila, Adrian Galdran, Estibaliz Garrote, and Joost Van de Weijer. Self-supervised blur detection from synthetically blurred scenes. *Image and Vision Computing*, 92:103804, 2019. 3
- [2] Ali Jahani Amiri, Shing Yan Loo, and Hong Zhang. Semi-supervised monocular depth estimation with left-right consistency using deep neural network. In *ROBIO*, pages 602–607, 2019. 2
- [3] Philip Bachman, Ouais Alsharif, and Doina Precup. Learning with pseudo-ensembles. *NIPS*, 27, 2014. 2
- [4] Roman Bachmann, David Mizrahi, Andrei Atanov, and Amir Zamir. Multimae: Multi-modal multi-task masked autoencoders. *arXiv*, 2022. 4
- [5] Jongbeom Baek, Gyeongnyeon Kim, and Seungryong Kim. Semi-supervised learning with mutual distillation for monocular depth estimation. *arXiv*, 2022. 1
- [6] Hangbo Bao, Li Dong, and Furu Wei. Beit: Bert pre-training of image transformers. *arXiv*, 2021. 2, 3, 4
- [7] David Berthelot, Nicholas Carlini, Ekin D Cubuk, Alex Kurakin, Kihyuk Sohn, Han Zhang, and Colin Raffel. Remixmatch: Semi-supervised learning with distribution alignment and augmentation anchoring. *arXiv*, 2019. 3
- [8] David Berthelot, Nicholas Carlini, Ian Goodfellow, Nicolas Papernot, Avital Oliver, and Colin A Raffel. Mixmatch: A holistic approach to semi-supervised learning. *NIPS*, 32, 2019. 1, 3
- [9] Amlaan Bhoi. Monocular depth estimation: A survey. *arXiv preprint arXiv:1901.09402*, 2019. 2
- [10] Jiawang Bian, Zhichao Li, Naiyan Wang, Huangying Zhan, Chunhua Shen, Ming-Ming Cheng, and Ian Reid. Unsupervised scale-consistent depth and ego-motion learning from monocular video. *Advances in neural information processing systems*, 32, 2019. 2
- [11] Po-Yi Chen, Alexander H Liu, Yen-Cheng Liu, and Yu-Chiang Frank Wang. Towards scene understanding: Unsupervised monocular depth estimation with semantic-aware representation. In *CVPR*, pages 2624–2632, 2019. 3
- [12] Xinlei Chen and Kaiming He. Exploring simple siamese representation learning. In *CVPR*, pages 15750–15758, 2021. 6
- [13] Jaehoon Cho, Dongbo Min, Youngjung Kim, and Kwanghoon Sohn. A large rgb-d dataset for semi-supervised monocular depth estimation. *arXiv*, 2019. 2, 3
- [14] Hyesong Choi, Hunsang Lee, Sunkyung Kim, Sunok Kim, Seungryong Kim, Kwanghoon Sohn, and Dongbo Min. Adaptive confidence thresholding for monocular depth estimation. In *ICCV*, pages 12808–12818, 2021. 1, 2
- [15] Marius Cordts, Mohamed Omran, Sebastian Ramos, Timo Rehfeld, Markus Enzweiler, Rodrigo Benenson, Uwe Franke, Stefan Roth, and Bernt Schiele. The cityscapes dataset for semantic urban scene understanding. In *CVPR*, pages 3213–3223, 2016. 7
- [16] Jia Deng, Wei Dong, Richard Socher, Li-Jia Li, Kai Li, and Li Fei-Fei. Imagenet: A large-scale hierarchical image database. In *CVPR*, pages 248–255. Ieee, 2009. 6
- [17] Jacob Devlin, Ming-Wei Chang, Kenton Lee, and Kristina Toutanova. Bert: Pre-training of deep bidirectional transformers for language understanding. *arXiv*, 2018. 3
- [18] Terrance DeVries and Graham W Taylor. Improved regularization of convolutional neural networks with cutout. *arXiv*, 2017. 4, 7
- [19] Alexey Dosovitskiy, Lucas Beyer, Alexander Kolesnikov, Dirk Weissenborn, Xiaohua Zhai, Thomas Unterthiner, Mostafa Dehghani, Matthias Minderer, Georg Heigold, Sylvain Gelly, et al. An image is worth 16x16 words: Transformers for image recognition at scale. *arXiv*, 2020. 3, 4, 14
- [20] Debidatta Dwivedi, Ishan Misra, and Martial Hebert. Cut, paste and learn: Surprisingly easy synthesis for instance detection. In *ICCV*, pages 1301–1310, 2017. 6
- [21] David Eigen, Christian Puhrsch, and Rob Fergus. Depth map prediction from a single image using a multi-scale deep network. *NIPS*, 27, 2014. 1, 2, 3, 6
- [22] Geoff French, Timo Aila, Samuli Laine, Michal Mackiewicz, and Graham Finlayson. Semi-supervised semantic segmentation needs strong, high-dimensional perturbations. 2019. 1, 3
- [23] Adrien Gaidon, Qiao Wang, Yohann Cabon, and Eleonora Vig. Virtual worlds as proxy for multi-object tracking analysis. In *Proceedings of the IEEE conference on computer vision and pattern recognition*, pages 4340–4349, 2016. 8
- [24] Ravi Garg, BG Vijay Kumar, Gustavo Carneiro, and Ian Reid. Unsupervised cnn for single view depth estimation: Geometry to the rescue. In *ECCV*, pages 740–756. Springer, 2016. 2, 3, 5, 7
- [25] Andreas Geiger, Philip Lenz, and Raquel Urtasun. Are we ready for autonomous driving? the kitti vision benchmark suite. In *CVPR*, pages 3354–3361. IEEE, 2012. 1, 2, 3, 6, 7, 8, 9, 10, 11, 14
- [26] Golnaz Ghiasi, Yin Cui, Aravind Srinivas, Rui Qian, Tsung-Yi Lin, Ekin D Cubuk, Quoc V Le, and Barret Zoph. Simple copy-paste is a strong data augmentation method for instance segmentation. In *CVPR*, pages 2918–2928, 2021. 6
- [27] Spyros Gidaris, Praveer Singh, and Nikos Komodakis. Unsupervised representation learning by predicting image rotations. *arXiv*, 2018. 4
- [28] Clément Godard, Oisín Mac Aodha, and Gabriel J Brostow. Unsupervised monocular depth estimation with left-right consistency. In *CVPR*, pages 270–279, 2017. 1, 2, 3
- [29] Clément Godard, Oisín Mac Aodha, Michael Firman, and Gabriel J Brostow. Digging into self-supervised monocular depth estimation. In *ICCV*, pages 3828–3838, 2019. 1, 2, 5, 7
- [30] Jean-Bastien Grill, Florian Strub, Florent Altché, Corentin Tallec, Pierre Richemond, Elena Buchatskaya, Carl Doersch, Bernardo Avila Pires, Zhaohan Guo, Mohammad Gheshlaghi Azar, et al. Bootstrap your own latent—a new approach to self-supervised learning. *NIPS*, 33:21271–21284, 2020. 6
- [31] Xiaoyang Guo, Hongsheng Li, Shuai Yi, Jimmy Ren, and Xiaogang Wang. Learning monocular depth by distilling cross-domain stereo networks. In *ECCV*, pages 484–500, 2018. 2, 3

- [32] Kaiming He, Xinlei Chen, Saining Xie, Yanghao Li, Piotr Dollár, and Ross Girshick. Masked autoencoders are scalable vision learners. *arXiv*, 2021. [2](#), [3](#), [4](#), [7](#)
- [33] Jingwei Huang, Zhili Chen, Duygu Ceylan, and Hailin Jin. 6-dof vr videos with a single 360-camera. In *VR*, pages 37–44. IEEE, 2017. [1](#)
- [34] Yasunori Ishii and Takayoshi Yamashita. Cutdepth: Edge-aware data augmentation in depth estimation. *arXiv*, 2021. [1](#)
- [35] Alex Kendall and Yarin Gal. What uncertainties do we need in bayesian deep learning for computer vision? *NIPS*, 30, 2017. [2](#), [4](#), [5](#), [6](#)
- [36] Doyeon Kim, Woonghyun Ga, Pyungwhan Ahn, Donggyu Joo, Sehwan Chun, and Junmo Kim. Global-local path networks for monocular depth estimation with vertical cutdepth. *arXiv*, 2022. [1](#)
- [37] Seungryong Kim, Kihong Park, Kwanghoon Sohn, and Stephen Lin. Unified depth prediction and intrinsic image decomposition from a single image via joint convolutional neural fields. In *ECCV*, pages 143–159, 2016. [1](#), [3](#)
- [38] Solomon Kullback. *Information theory and statistics*. Courier Corporation, 1997. [4](#)
- [39] Varun Ravi Kumar, Sandesh Athni Hiremath, Markus Bach, Stefan Milz, Christian Witt, Clément Pinard, Senthil Yogamani, and Patrick Mäder. Fisheyedistancenet: Self-supervised scale-aware distance estimation using monocular fisheye camera for autonomous driving. In *ICRA*, pages 574–581. IEEE, 2020. [1](#)
- [40] Jogendra Nath Kundu, Phani Krishna Uppala, Anuj Pahuja, and R Venkatesh Babu. Adadept: Unsupervised content congruent adaptation for depth estimation. In *Proceedings of the IEEE conference on computer vision and pattern recognition*, pages 2656–2665, 2018. [8](#)
- [41] Chia-Wen Kuo, Chih-Yao Ma, Jia-Bin Huang, and Zsolt Kira. Featmatch: Feature-based augmentation for semi-supervised learning. In *ECCV*, pages 479–495. Springer, 2020. [3](#)
- [42] Yevhen Kuznietsov, Jorg Stuckler, and Bastian Leibe. Semi-supervised deep learning for monocular depth map prediction. In *CVPR*, pages 6647–6655, 2017. [2](#), [3](#)
- [43] Lubor Ladicky, Jianbo Shi, and Marc Pollefeys. Pulling things out of perspective. In *CVPR*, pages 89–96, 2014. [2](#)
- [44] Samuli Laine and Timo Aila. Temporal ensembling for semi-supervised learning. *arXiv*, 2016. [1](#), [2](#), [4](#)
- [45] Wonwoo Lee, Nohyoung Park, and Woontack Woo. Depth-assisted real-time 3d object detection for augmented reality. In *ICAT*, volume 11, pages 126–132, 2011. [1](#)
- [46] Bo Li, Chunhua Shen, Yuchao Dai, Anton Van Den Hengel, and Mingyi He. Depth and surface normal estimation from monocular images using regression on deep features and hierarchical crfs. In *CVPR*, pages 1119–1127, 2015. [1](#), [2](#)
- [47] Zhenyu Li, Zehui Chen, Xianming Liu, and Junjun Jiang. Depthformer: Exploiting long-range correlation and local information for accurate monocular depth estimation. *arXiv*, 2022. [3](#)
- [48] Luke Melas-Kyriazi and Arjun K Manrai. Pixmatch: Unsupervised domain adaptation via pixelwise consistency training. In *Proceedings of the IEEE/CVF Conference on Computer Vision and Pattern Recognition*, pages 12435–12445, 2021. [8](#)
- [49] Takeru Miyato, Shin-ichi Maeda, Masanori Koyama, and Shin Ishii. Virtual adversarial training: a regularization method for supervised and semi-supervised learning. *PAMI*, 41(8):1979–1993, 2018. [4](#)
- [50] Yassine Ouali, Céline Hudelot, and Myriam Tami. Semi-supervised semantic segmentation with cross-consistency training. In *CVPR*, pages 12674–12684, 2020. [1](#)
- [51] Adam Paszke, Sam Gross, Soumith Chintala, Gregory Chanan, Edward Yang, Zachary DeVito, Zeming Lin, Alban Desmaison, Luca Antiga, and Adam Lerer. Automatic differentiation in pytorch. 2017. [6](#)
- [52] Deepak Pathak, Philipp Krahenbuhl, Jeff Donahue, Trevor Darrell, and Alexei A Efros. Context encoders: Feature learning by inpainting. In *CVPR*, pages 2536–2544, 2016. [2](#), [5](#)
- [53] Andrea Pilzer, Stephane Lathuiliere, Nicu Sebe, and Elisa Ricci. Refine and distill: Exploiting cycle-inconsistency and knowledge distillation for unsupervised monocular depth estimation. In *CVPR*, pages 9768–9777, 2019. [3](#)
- [54] Koutilya PNVN, Hao Zhou, and David Jacobs. Sharingan: Combining synthetic and real data for unsupervised geometry estimation. In *Proceedings of the IEEE/CVF Conference on Computer Vision and Pattern Recognition*, pages 13974–13983, 2020. [8](#)
- [55] Matteo Poggi, Filippo Aleotti, Fabio Tosi, and Stefano Mattoccia. On the uncertainty of self-supervised monocular depth estimation. In *CVPR*, pages 3227–3237, 2020. [2](#), [4](#)
- [56] René Ranftl, Alexey Bochkovskiy, and Vladlen Koltun. Vision transformers for dense prediction. In *ICCV*, pages 12179–12188, 2021. [3](#), [4](#), [6](#), [7](#), [14](#)
- [57] Mehdi Sajjadi, Mehran Javanmardi, and Tolga Tasdizen. Regularization with stochastic transformations and perturbations for deep semi-supervised learning. *NIPS*, 29, 2016. [1](#), [2](#), [4](#)
- [58] Ashutosh Saxena, Sung H Chung, and Andrew Y Ng. 3-d depth reconstruction from a single still image. *IJCV*, 76(1):53–69, 2008. [2](#)
- [59] Nathan Silberman, Derek Hoiem, Pushmeet Kohli, and Rob Fergus. Indoor segmentation and support inference from rgbd images. In *ECCV*, pages 746–760. Springer, 2012. [1](#), [2](#), [3](#), [6](#), [9](#), [10](#), [14](#)
- [60] Kihyuk Sohn, David Berthelot, Nicholas Carlini, Zizhao Zhang, Han Zhang, Colin A Raffel, Ekin Dogus Cubuk, Alexey Kurakin, and Chun-Liang Li. Fixmatch: Simplifying semi-supervised learning with consistency and confidence. *NIPS*, 33:596–608, 2020. [1](#), [2](#), [3](#), [6](#)
- [61] Shuran Song, Samuel P Lichtenberg, and Jianxiong Xiao. Sun rgb-d: A rgb-d scene understanding benchmark suite. In *Proceedings of the IEEE conference on computer vision and pattern recognition*, pages 567–576, 2015. [7](#)
- [62] Antti Tarvainen and Harri Valpola. Mean teachers are better role models: Weight-averaged consistency targets improve semi-supervised deep learning results. *NIPS*, 30, 2017. [1](#), [3](#)

- [63] Alessio Tonioni, Matteo Poggi, Stefano Mattoccia, and Luigi Di Stefano. Unsupervised domain adaptation for depth prediction from images. *PAMI*, 42(10):2396–2409, 2019. 3
- [64] Fabio Tosi, Filippo Aleotti, Matteo Poggi, and Stefano Mattoccia. Learning monocular depth estimation infusing traditional stereo knowledge. In *CVPR*, pages 9799–9809, 2019. 2
- [65] Jonas Uhrig, Nick Schneider, Lukas Schneider, Uwe Franke, Thomas Brox, and Andreas Geiger. Sparsity invariant cnns. In *3DV*, pages 11–20. IEEE, 2017. 3, 6, 9
- [66] Benjamin Ummerhofer, Huizhong Zhou, Jonas Uhrig, Nikolaus Mayer, Eddy Ilg, Alexey Dosovitskiy, and Thomas Brox. Demon: Depth and motion network for learning monocular stereo. In *CVPR*, pages 5038–5047, 2017. 1, 2
- [67] Chaoyang Wang, José Miguel Buenaposada, Rui Zhu, and Simon Lucey. Learning depth from monocular videos using direct methods. In *Proceedings of the IEEE conference on computer vision and pattern recognition*, pages 2022–2030, 2018. 2
- [68] Lijun Wang, Yifan Wang, Linzhao Wang, Yunlong Zhan, Ying Wang, and Huchuan Lu. Can scale-consistent monocular depth be learned in a self-supervised scale-invariant manner? In *Proceedings of the IEEE/CVF International Conference on Computer Vision*, pages 12727–12736, 2021. 2
- [69] Xiaolong Wang, David Fouhey, and Abhinav Gupta. Designing deep networks for surface normal estimation. In *CVPR*, pages 539–547, 2015. 3
- [70] Zhou Wang and Alan C Bovik. Mean squared error: Love it or leave it? a new look at signal fidelity measures. *IEEE signal processing magazine*, 26(1):98–117, 2009. 4
- [71] Jamie Watson, Michael Firman, Gabriel J Brostow, and Daniyar Turmukhambetov. Self-supervised monocular depth hints. In *ICCV*, pages 2162–2171, 2019. 2, 3
- [72] Junyuan Xie, Ross Girshick, and Ali Farhadi. Deep3d: Fully automatic 2d-to-3d video conversion with deep convolutional neural networks. In *ECCV*, pages 842–857. Springer, 2016. 2, 3
- [73] Qizhe Xie, Zihang Dai, Eduard Hovy, Thang Luong, and Quoc Le. Unsupervised data augmentation for consistency training. *NIPS*, 33:6256–6268, 2020. 2, 3
- [74] Zhenda Xie, Zheng Zhang, Yue Cao, Yutong Lin, Jianmin Bao, Zhuliang Yao, Qi Dai, and Han Hu. Simmim: A simple framework for masked image modeling. *arXiv*, 2021. 2, 3, 4, 7
- [75] Haohang Xu, Shuangrui Ding, Xiaopeng Zhang, Hongkai Xiong, and Qi Tian. Masked autoencoders are robust data augmentors. *arXiv preprint arXiv:2206.04846*, 2022. 3
- [76] Guanglei Yang, Hao Tang, Mingli Ding, Nicu Sebe, and Elisa Ricci. Transformer-based attention networks for continuous pixel-wise prediction. In *ICCV*, pages 16269–16279, 2021. 3
- [77] Zhichao Yin and Jianping Shi. Geonet: Unsupervised learning of dense depth, optical flow and camera pose. In *CVPR*, pages 1983–1992, 2018. 3
- [78] Senthil Yogamani, Ciarán Hughes, Jonathan Horgan, Ganesh Sistu, Pdraig Varley, Derek O’Dea, Michal Uricár, Stefan Milz, Martin Simon, Karl Amende, et al. Woodscape: A multi-task, multi-camera fisheye dataset for autonomous driving. In *Proceedings of the IEEE/CVF International Conference on Computer Vision*, pages 9308–9318, 2019. 1
- [79] Chaoning Zhang, Kang Zhang, Chenshuang Zhang, Trung X Pham, Chang D Yoo, and In So Kweon. How does simsim avoid collapse without negative samples? a unified understanding with self-supervised contrastive learning. *arXiv*, 2022. 6, 8
- [80] Shanshan Zhao, Huan Fu, Mingming Gong, and Dacheng Tao. Geometry-aware symmetric domain adaptation for monocular depth estimation. In *Proceedings of the IEEE/CVF Conference on Computer Vision and Pattern Recognition*, pages 9788–9798, 2019. 8
- [81] Chuanxia Zheng, Tat-Jen Cham, and Jianfei Cai. T2net: Synthetic-to-realistic translation for solving single-image depth estimation tasks. In *Proceedings of the European Conference on Computer Vision (ECCV)*, pages 767–783, 2018. 8
- [82] Tinghui Zhou, Matthew Brown, Noah Snavely, and David G Lowe. Unsupervised learning of depth and ego-motion from video. In *CVPR*, pages 1851–1858, 2017. 1, 3
- [83] Yuliang Zou, Zizhao Zhang, Han Zhang, Chun-Liang Li, Xiao Bian, Jia-Bin Huang, and Tomas Pfister. Pseudoseg: Designing pseudo labels for semantic segmentation. *arXiv*, 2020. 1, 3